Transp Porous Med (2014) 105:191–209
DOI 10.1007/s11242-014-0366-8

Diffusive Effects on Recovery of Light Oil by Medium Temperature Oxidation

Negar Khoshnevis Gargar · Alexei A. Mailybaev · Dan Marchesin · Hans Bruining

Received: 13 May 2013 / Accepted: 17 July 2014 / Published online: 2 August 2014

Abstract Volatile oil recovery by means of air injection is studied as a method to improve recovery from low permeable reservoirs. We consider the case in which the oil is directly combusted into small products, for which we use the term medium temperature oil combustion. The two-phase model considers evaporation, condensation and reaction with oxygen. In the absence of thermal, molecular and capillary diffusion, the relevant transport equations can be solved analytically. The solution consists of three waves, i.e., a thermal wave, a medium temperature oxidation (MTO) wave and a saturation wave separated by constant state regions. A striking feature is that evaporation occurs upstream of the combustion reaction in the MTO wave. The purpose of this paper is to show the effect of diffusion mechanisms on the MTO process. We used a finite element package (COMSOL) to obtain a numerical solution; the package uses fifth-order Lagrangian base functions, combined with a central difference scheme. This makes it possible to model situations at realistic diffusion coefficients. The qualitative behavior of the numerical solution is similar to the analytical solution. Molecular diffusion lowers the temperature of the MTO wave, but creates a small peak near the vaporization region. The effect of thermal diffusion smoothes the thermal wave and widens the MTO region. Capillary diffusion increases the temperature in the upstream part of the MTO region and decreases the efficiency of oil recovery. At increasing capillary diffusion the

N. Khoshnevis Gargar (✉) · H. Bruining
Civil Engineering and Geosciences, Delft University of Technology,
Stevinweg 1, 2628 CE Delft, The Netherlands
e-mail: n.khoshnevisgargar@tudelft.nl

H. Bruining
e-mail: j.bruining@tudelft.nl

A. A. Mailybaev · D. Marchesin
Instituto Nacional de Matemática Pura e Aplicada (IMPA), Estrada Dona Castorina 110,
Rio de Janeiro 22460-320, Brazil
e-mail: alexei@impa.br

D. Marchesin
e-mail: marchesi@impa.br

recovery by gas displacement gradually becomes higher, leaving less oil to be recovered by combustion. Consequently, the analytical solution with no diffusion and numerical solutions at a high capillary diffusion coefficient become different. Therefore high numerical diffusion, significant in numerical simulations especially in coarse gridded simulations, may conceal the importance of combustion in recovering oil.

Keywords Air Injection · Medium temperature oxidation · Diffusive effects · Light oil recovery · In-situ combustion

List of Symbols

A_r	MTO reaction pre-exponential factor (1/s)
c_l, c_g	Heat capacity of liquid and gas (J/mol K)
C_m	Heat capacity of porous matrix (J/m^3 K)
D_g	Gas-diffusion coefficient (m^2/s)
f_l	Fractional flow function for liquid phase
J	Leverett J-function
k	Rock permeability (m^2)
k_l, k_g	Liquid and gas phase permeabilities (m^2)
n	MTO Reaction order with respect to oxygen
P_g	Gas pressure (Pa)
P_l	Liquid pressure (Pa)
Q_r	MTO reaction enthalpy per mole of oxygen at reservoir temperature (J/mol)
Q_v	Liquid fuel vaporization heat at reservoir temperature (J/mol)
R	Ideal gas constant (J/(mol K)
s_l, s_g	Saturations of liquid and gas phases
t	Time (s)
T	Temperature (K)
T^b	Boiling temperature of liquid at elevated pressure (K)
T^ini	Reservoir temperature (K)
T^ac	MTO activation temperature (K)
u_l, u_g, u	Liquid, gas and total Darcy velocities (m/s)
u_gj	Darcy velocity of component $j = h, o, r$ in gas phase (m/s)
$u_\mathrm{g}^\mathrm{inj}$	Injection Darcy velocity of gas (m/s)
W_v, W_r	Vaporization rate, and MTO reaction rate (mol/m^3 s)
x	Spatial coordinate (m)
Y_h, Y_o, Y_r	Gas molar fractions: hydrocarbons, oxygen, remaining components (mol/mol)
$Y_\mathrm{o}^\mathrm{inj}$	Oxygen fraction in injected gas
φ	porosity
κ_l	Phase transfer parameter
λ	Thermal conductivity of porous medium (W/m K)
μ_l, μ_g	Viscosity of liquid and gas (Pa s)
ν_l, ν_g	Stoichiometric coefficients in the MTO reaction
ρ_l, ρ_g	Molar densities of liquid and gas (mol/m^3)
σ	Liquid oil surface tension (N/m)
θ	Liquid oil/rock contact angle

1 Introduction

Reactive transport in porous media is important for a variety of processes that cover the range from small-scale reaction-diffusion problems in catalyst pellets to large-scale transport problems in geologic reservoirs; one example is in-situ combustion (ISC), also referred to as fire flood. In view of the decline of easy oil and the difficulties encountered in the production of heavy oil, ISC and high pressure air injection (HPAI) are considered as effective ways to enhance the recovery of oil. In these cases the oxygen in the injected air reacts with the heavier components of the oil, generating a hot zone in which cracking and vaporization of lighter components occur. Air injection has the advantage of air availability at any location (Schulte 2005); however, energy costs of air compression, necessary for injection, are not negligible (Eftekhari et al. 2012). Oil combustion is generally not only considered as a technique that is applicable for heavy oils because of the conspicuous reduction in oil viscosity due to the generated heat, but it also promotes production through thermal expansion, distillation, and gas drive caused by combustion gases. The air injection process is often referred to as high pressure air injection when it is applied to deep light oil reservoirs, whereas the term in-situ combustion has been traditionally used for heavy oil reservoirs. The mechanism actually responsible for oil displacement in ISC varies with the type of oil. For light oil, evaporation and condensation are just as important as the oxidation reaction (Mailybaev et al. 2013). As opposed to heavy oil combustion, light oil combustion occurs usually at lower temperatures because the oil is only partially oxidized. When evaporation is small and locally all of the light oil is oxidized, relatively high temperatures can still occur. Thermal and mass diffusion as well as capillary forces lead to diffusive processes and are important when steep changes occur in the dependent variables in the wave profile. It is the purpose of this work to determine the effects of capillary pressure diffusion, longitudinal heat conduction, and mass diffusion on the combustion recovery process.

Combustion for low and medium viscosity oil (Abou-Kassem et al. 1986; Akin et al. 2000; Bruining et al. 2009; Castanier and Brigham 1997, 2003; Kok and Karacan 2000; Lin et al. 1987, 1984; Xu et al. 2004) is described by different mechanisms. For light oil combustion, coke formation is usually disregarded, although it can occur (Khoshnevis Gargar et al. 2010). At lower temperatures, the crude oil undergoes the oxidation reaction without generating carbon mono- and dioxide. As the temperature rises, distillation coupled with pyrolysis produces hydrogen gas and some light hydrocarbons in the gas phase. A major part of these hydrocarbons are produced without undergoing oxidation (Fassihi et al. 1984). However, oxygen reacts with the remainder of these hydrocarbons and therefore medium temperature oxidation occurs. Further increase of temperature leads first to deposition and then to combustion of coke.

In summary we have high temperature oxidation (HTO) when heat conducted out of the reaction zone converts the oil to coke before it is combusted, low temperature oxidation (LTO) when the oxygen is incorporated in the hydrocarbon molecules to form alcohols, aldehydes, acids, or other oxygenated hydrocarbons (Greaves et al. 2000a, b; Hardy et al. 1972), and medium temperature oxidation (MTO) (Greaves et al. 2000b; Gutierrez et al. 2009; Germain and Geyelin 1997) when the oxidation reaction leads to scission of the molecules and formation of small reaction products such as water, CO, or CO_2. The focus of this paper is on MTO.

ISC is a complex process that involves the interaction of many physical phenomena that occur at different time and space scales. Indeed, one of the reasons for difficulty in simulating ISC is the disparity in time and space scales at which the dominant mechanisms occur. For instance, the time and space scales associated with advection or heat conduction are much

larger than the scales at which chemical reactions happen in the reservoir, which in turn are considered larger than the scales associated with the transfer of components between phases (Gerritsen et al. 2004). Only at fine temporal and spatial grid step sizes, the impact of numerical errors may be sufficiently reduced to give reasonable predictions of combustion, saturation, and heat wave speed. To establish this unambiguously, it is important to compare numerical computations with results from models that allow analytical solutions (Whitham 1967, 2011).

There are many papers presenting the results of numerical simulation of combustion tube experiments. These papers deal with the kinetics of the reactions for light and heavy oil (Lin et al. 1984) and focus less on the evaporation and condensation mechanisms. In most of these papers, the thermal, mass diffusion, and capillary forces are disregarded. However, in some works thermal diffusion is included (Adagülü and Akkutlu 2007). In the continuity equations for the components, molecular diffusion has not been explicitly considered (Belgrave and Moore 1992) in view of the dominating effect of numerical diffusion introduced by the finite-difference approximations (Von Rosenberg 1969; Peaceman 1977).

The mathematical theory of combustion in porous media is well developed for immobile fuels, e.g., Bayliss and Matkowsky (1994); Bruining et al. (2009); Matkowsky and Sivashinsky (1978); Schult et al. (1996); Wahle et al. (2003); Mailybaev et al. (2011). When the fuel is a mobile liquid and, additionally, undergoes gas-liquid phase transitions, the problem becomes more complicated. It was shown in Mailybaev et al. (2011) that, in the case of liquid fuel, the combustion wave has a resonant structure similar to that encountered earlier in detonation problems, see Fickett and Davis (2011); Kulikovskii and Pashchenko (2005); Sharpe and Falle (2000); Wood and Salsburg (1960). In this case at some point in the internal structure of the wave (resonant point), the Buckley–Leverett characteristic speed is equal to the combustion wave velocity. In this resonant case, analysis of the internal wave structure (i.e., the reaction zone) is necessary in order to obtain macroscopic parameters of the wave. However, the determining equations appear to be independent of the particular form of the evaporation and reaction rate expressions, as vaporization is usually much faster than combustion.

In this paper we consider exclusively modeling and simulation of the MTO combustion process. We examine a simplified model for light oil recovery by air injection in the absence of water, but including mass-, thermal-, and capillary diffusion for air injection in light oil reservoirs, leading to medium temperature oxidation. This is an extension of the model suggested in Mailybaev et al. (2013), which is given by a system of multi-phase flow balance equations with source terms describing reaction and vaporization rates, and an energy balance equation. Despite the fact that water is important in thermal processes, sometimes increasing the oil production (Dietz and Weijdema 1968),we are not yet considering in the current work water that may be present initially or that condenses from steam originating from the reaction. We consider only a one-component oil, e.g., heptane in dry porous rock, to improve the understanding of the oxidation/evaporation/condensation mechanisms and include diffusive processes to allow comparison to the non-diffusive process, which can be solved analytically (Mailybaev et al. 2013). Heptane represents a single pseudo-component as liquid fuel, which is characterized by an average boiling temperature, density, and viscosity. It turns out that the oxidation, evaporation, and condensation often occur at locations close to each other that move with the same speed in the porous medium (Mailybaev et al. 2013). The temperature variation is bounded by the oil boiling temperature and thus not very large. The presence of liquid fuel, which is mobile and can vaporize or condense, is a challenge for modeling the combustion process. We consider only the one-dimensional problem, expecting that its

solution contributes to understanding of the MTO processes (Greaves et al. 2000b; Germain and Geyelin 1997; Gutierrez et al. 2009) that occur in practice.

The paper is organized as follows. The model is introduced in Sect. 2. Section 3 describes the analytical solution for the non-diffusive model. Section 4 presents the numerical results for thermal, capillary, and mass diffusive processes. We end with some conclusions.

2 Model

We study a two-phase flow problem involving a combustion front when air is injected into porous rock filled with light oil. The temperature of the medium is bounded by the boiling point of the liquid and, thus, remains relatively low. There are numerous references indicating that gas-phase reactions in porous media in itself are important (Bakry et al. 2011; Pereira et al. 2009; Sanmiguel et al. 2002; Zheng et al. 2010). Gas-phase reactions can be important for HPAI (Barzin et al. 2010). We disregard gas-phase reactions, because there are also many references that indicate that gas-phase reactions in in-situ combustion play a minor role (Barzin et al. 2010) with respect to the reactions with liquid or solid fuel. In summary, it is still a matter of debate whether gas-phase reactions play a significant role in porous media as annihilation of free radicals at the pore walls will drastically reduce the reaction rates (Bamford 1977; Helfferich 2004; Levenspiel 1999; Schott 1960; Fisher et al. 2000).

When oxygen reacts with liquid hydrocarbons at low temperatures, a series of reactions may occur that convert hydrocarbons into oxygenated hydrocarbons (ketones, alcohols, aldehydes, and acids). Further oxidation leads eventually to complete combustion of the oxygenated hydrocarbons (Fisher et al. 2000); in this paper, the combined reaction to oxygenated hydrocarbons and the subsequent reaction to gaseous products are simplified into the form of a single reaction modeled as

$$\nu_{\mathrm{l}}(\text{hydrocarbons}) + \mathrm{O}_2 \rightarrow \nu_g\,(\text{gaseous products}), \tag{2.1}$$

i.e., one mole of oxygen reacts with ν_{l} moles of initial (liquid) hydrocarbons generating ν_{g} moles of gaseous products (H_2O, CO_2, etc.). This system is studied in one dimension (flow in the positive spatial direction x), allowing for the presence of oil and gas. The liquid saturation is denoted by s_{l} and the gas saturation is $s_{\mathrm{g}} = 1 - s_{\mathrm{l}}$. In the gaseous phase, we distinguish the molar fraction of hydrocarbon gas Y_{h} and the molar fraction of oxygen Y_{o}. The remaining components with molar fraction $Y_{\mathrm{r}} = 1 - Y_{\mathrm{o}} - Y_{\mathrm{h}}$ consist of reaction products and inert components from the injected gas. The molar mass balance equations for liquid and gas components are

$$\partial_t(\varphi\rho_{\mathrm{l}}s_l) + \partial_x(\rho_{\mathrm{l}}u_l) = -\nu_l W_r - W_{\mathrm{v}}, \tag{2.2}$$

$$\partial_t(\varphi Y_{\mathrm{h}}\rho_{\mathrm{g}}s_g) + \partial_x(\rho_{\mathrm{g}}u_{gh}) = W_{\mathrm{v}}, \tag{2.3}$$

$$\partial_t(\varphi Y_{\mathrm{o}}\rho_{\mathrm{g}}s_g) + \partial_x(\rho_{\mathrm{g}}u_{go}) = -W_r, \tag{2.4}$$

$$\partial_t(\varphi Y_{\mathrm{r}}\rho_{\mathrm{g}}s_g) + \partial_x(\rho_{\mathrm{g}}u_{gr}) = \nu_g W_r, \tag{2.5}$$

where $u_{\alpha j}$ means the Darcy velocity of component j in phase α . There are three components, viz., gaseous hydrocarbon (h), oxygen (o), and the "rest" (r) in the gas phase. Light oil can exist in the liquid phase l and the gas phase g, whereas oxygen and the rest can only exist in the gas phase. The liquid, gas, and total Darcy velocities are

$$u_{\mathrm{l}} = -\frac{k_{\mathrm{l}}}{\mu_l}\frac{\partial P_{\mathrm{l}}}{\partial x}, \quad u_{\mathrm{g}} = -\frac{k_{\mathrm{g}}}{\mu_g}\frac{\partial P_{\mathrm{g}}}{\partial x}, \quad u = u_{\mathrm{g}} + u_{\mathrm{l}}. \tag{2.6}$$

In this equation $\mu_l(T)$ and $\mu_g(T)$ are the viscosities, P_l is the oil pressure, and P_g is the gas pressure. We denote the permeability of phase α by k_α. We disregard the effect of capillary forces on the phase behavior. Moreover, we also disregard pressure variations due to fluid flow on the density and thermodynamic behavior. We use the ideal gas law to relate the molar density ρ_g to the pressure P_g, i.e.,

$$\rho_g = \frac{P_g}{RT}. \tag{2.7}$$

The capillary pressure $P_c(s_l) = P_g - P_l$ is given by

$$P_c(s_l) = \frac{\sigma \cos(\theta)}{\sqrt{k/\varphi}} J(s_l), \tag{2.8}$$

where the factor multiplying the Leverett J-function is constant (Bear, 1972, p. 445-446). We will use the derivative of Eq. (2.8) to estimate the order of magnitude of the capillary diffusion coefficient; however, we will assume a saturation-independent average value. It is convenient to express the liquid and gas velocities as

$$u_l = u f_l + \frac{f_g k_l}{\mu_l} P_c'(s_l) \frac{\partial s_l}{\partial x}, \quad u_g = u - u_l, \tag{2.9}$$

where the prime denotes the derivative with respect to the function argument, and the liquid and gas fractional flow functions are

$$f_l(s_l, T) = \frac{k_l/\mu_l}{k_l/\mu_l + k_g/\mu_g}, \quad f_g = 1 - f_l. \tag{2.10}$$

The Darcy velocities for gas components are

$$u_{gj} = Y_j u_g - \varphi D_g s_g \partial_x(Y_j) \quad (j = h, o, r). \tag{2.11}$$

As a first approximation, we use the same diffusion coefficient D_g for all gas components (see, however, the Stefan–Maxwell relations in Bird et al. (2002) for the full composition dependence).

The permeability functions for the liquid phase and gas phase are taken as

$$k_l(s_l) = k \left(\frac{s_l - s_{lr}}{1 - s_{lr}} \right)^2 \quad \text{for} \quad s_l \geq s_{lr}, \quad \text{and} \quad 0 \quad \text{otherwise}, \tag{2.12}$$

$$k_g(s_l) = k (1 - s_l)^3, \tag{2.13}$$

where we assume that the residual gas saturation is zero.

The temperature dependence of the gas and liquid viscosities μ_g and μ_l in cP is given as (Poling et al. 2001)

$$\mu_g = \frac{7.5}{T + 120} \left(\frac{T}{291} \right)^{3/2} \quad \text{and} \quad \mu_l = 1.32 \times 10^{-2} \exp\left(\frac{1,006}{T} \right). \tag{2.14}$$

By adding up (2.3)–(2.5) and using (2.11) with $Y_h + Y_o + Y_r = 1$, the total mass balance of the gases is given by

$$\partial_t(\varphi \rho_g s_g) + \partial_x(\rho_g u_g) = W_v + (v_g - 1) W_r. \tag{2.15}$$

Assuming that the temperature of solid rock, liquid, and gas is equal, we write the heat balance equation as

$$\frac{\partial}{\partial t}\left(C_{\mathrm{m}}+\varphi c_{\mathrm{l}}\rho_l s_{\mathrm{l}}+\varphi c_{\mathrm{g}}\rho_g s_{\mathrm{g}}\right)\Delta T + \frac{\partial}{\partial x}(c_{\mathrm{l}}\rho_l u_{\mathrm{l}}+c_{\mathrm{g}}\rho_g u_{\mathrm{g}})\Delta T = \lambda\frac{\partial^2 T}{\partial x^2}+Q_{\mathrm{r}}W_r-Q_{\mathrm{v}}W_v, \tag{2.16}$$

where $\Delta T = T - T^{ini}$ with initial reservoir temperature T^{ini}. The heat capacities for the sand matrix, the liquid phase, and gas phase are C_{m}, c_{l}, c_{g}, respectively; they are all assumed to be constant and independent of composition. We use λ to denote the effective thermal conductivity. We disregard heat losses, which are usually very small in field applications (however, taking into account heat losses become essential for interpreting laboratory experiments).

Our implementation for the liquid and gas Darcy velocities is described by

$$u_{\mathrm{l}} = -\frac{k_{\mathrm{l}}}{\mu_l}\frac{\partial P_{\mathrm{l}}}{\partial x} = -\frac{k_{\mathrm{l}}}{\mu_l}\frac{\partial(P_{\mathrm{g}}-P_c)}{\partial x} = -\frac{k_{\mathrm{l}}}{\mu_l}\frac{\partial P_{\mathrm{g}}}{\partial x} + \frac{k_{\mathrm{l}}}{\mu_l}\frac{\partial P_c}{\partial x} \approx -\frac{k_{\mathrm{l}}}{\mu_l}\frac{\partial P_{\mathrm{g}}}{\partial x} - D_{cap}\frac{\partial s_{\mathrm{l}}}{\partial x}, \tag{2.17}$$

in which we use the average value D_{cap} to avoid degenerate diffusion effects

$$D_{\mathrm{cap}} = -\int_0^1 \frac{k_{\mathrm{l}}}{\mu_l}\frac{\sigma\cos(\theta)}{\sqrt{k/\varphi}}J'(s_{\mathrm{l}})\mathrm{d}s_{\mathrm{l}}, \tag{2.18}$$

where the quantities are evaluated at the initial temperature T^{ini}, the parameters are given in Table 1 and we use typical values for the interfacial tension $\sigma \approx 0.03$ N/m and the contact angle $\theta = 0$. To estimate the capillary diffusion, it is assumed that the derivative of the Leverett J-function is equal to -0.3. Therefore, the capillary diffusion coefficient is estimated as $D_{\mathrm{cap}} = 1.0\times10^{-7}$ m^2/s. Then the mass balance equations (2.2)–(2.5) read

$$\begin{aligned}
\partial_t(\varphi\rho_{\mathrm{l}}s_l)+\partial_x(\rho_{\mathrm{l}}u_{ll})-\partial_x(D_{cap}\rho_{\mathrm{l}}\partial_x(s_{\mathrm{l}})) &= -\nu_{\mathrm{l}}W_{\mathrm{r}}-W_{\mathrm{v}}\,,\\
\partial_t(\varphi\rho_{\mathrm{g}}s_g)+\partial_x(\rho_{\mathrm{g}}u_g) &= W_{\mathrm{v}}+(\nu_{\mathrm{g}}-1)W_{\mathrm{r}}\,,\\
\partial_t(\varphi Y_{\mathrm{o}}\rho_{\mathrm{g}}s_g)+\partial_x(\rho_{\mathrm{g}}Y_{\mathrm{o}}u_g)-\partial_x(\varphi\rho_{\mathrm{g}}D_g s_g\partial_x(Y_{\mathrm{o}})) &= -W_{\mathrm{r}}\,,\\
\partial_t(\varphi Y_{\mathrm{r}}\rho_{\mathrm{g}}s_g)+\partial_x(\rho_{\mathrm{g}}Y_{\mathrm{r}}u_g)-\partial_x(\varphi\rho_{\mathrm{g}}D_g s_g\partial_x(Y_{\mathrm{r}})) &= \nu_{\mathrm{g}}W_{\mathrm{r}}\,,
\end{aligned} \tag{2.19}$$

where

$$u_{ll} = -\frac{k_{\mathrm{l}}}{\mu_l}\frac{\partial P_{\mathrm{g}}}{\partial x},\quad u_{\mathrm{l}} = u_{ll} - D_{cap}\frac{\partial s_{\mathrm{l}}}{\partial x}\,,\quad u_g = -\frac{k_{\mathrm{g}}}{\mu_g}\frac{\partial P_{\mathrm{g}}}{\partial x}. \tag{2.20}$$

The energy balance is given by

$$\partial_t((C_{\mathrm{m}}+\varphi c_{\mathrm{l}}\rho_l s_{\mathrm{l}}+\varphi c_{\mathrm{g}}\rho_g s_{\mathrm{g}})\Delta T)+\partial_x((c_{\mathrm{l}}\rho_l(u_{ll}-D_{\mathrm{cap}}\partial_x s_{\mathrm{l}}) + c_{\mathrm{g}}\rho_g u_{\mathrm{g}})\Delta T) = \lambda\frac{\partial^2 T}{\partial x^2}+Q_{\mathrm{r}}W_r-Q_{\mathrm{v}}W_v\,. \tag{2.21}$$

The partial pressure of the gaseous hydrocarbon in liquid-gas equilibrium is given by the Clausius–Clapeyron relation and Raoult's law as

$$Y_{\mathrm{h}}^{\mathrm{eq}} P_{\mathrm{g}} = P_{\mathrm{atm}} \exp\left(-\frac{Q_{\mathrm{v}}}{R}\left(\frac{1}{T} - \frac{1}{T^{\mathrm{bn}}}\right)\right), \tag{2.22}$$

where T^{bn} is the (normal) boiling point measured at atmospheric pressure P_{atm}. Taking $Y_{\mathrm{h}}^{\mathrm{eq}} = 1$ in (2.22), one recovers the actual boiling temperature $T = T^b$ at the elevated gas pressure $P_{\mathrm{g}} > P_{\mathrm{atm}}$. We can see that $Y_{\mathrm{h}}^{\mathrm{eq}}$ increases with temperature and $Y_{\mathrm{h}}^{\mathrm{eq}} \to 1$ as $T \to T^b$. Even if there are better boiling point relations than Clausius-Clapeyron [see Poling et al. (2001)], this relation is sufficiently accurate for our purpose.

We consider the reaction rate as

$$W_{\mathrm{r}} = A_r \varphi \rho_{\mathrm{l}} s_l \left(\frac{P_{\mathrm{g}} Y_{\mathrm{o}}}{P_{atm}}\right)^n \exp\left(-\frac{T^{ac}}{T}\right), \tag{2.23}$$

where A_r is the frequency factor for the oxidation rate of the oil. We use T^{ac} to denote the activation temperature for the oxidation rate. The activation temperature is related to the activation energy E_{ac} as $T^{\mathrm{ac}} = E_{\mathrm{ac}}/R$. We choose $T^{\mathrm{ac}} = 7066$ K.

We use an evaporation rate given by

$$W_{\mathrm{v}} = \kappa_{\mathrm{l}}(Y_{\mathrm{h}}^{eq} - Y_{\mathrm{h}})\rho_{\mathrm{g}} s_{\mathrm{l}}^{2/3}, \tag{2.24}$$

where we assume that the evaporation rate is proportional to the deviation of the mole fraction of the light oil component in the gas phase from its equilibrium value and proportional to $s_{\mathrm{l}}^{2/3}$, which is related to the surface area. The empirical transfer parameter is denoted as κ_{l}. This formulation can be considered a consequence of non-equilibrium thermodynamics [see for instance (Prigogine 1962; Levenspiel 1999)]. If κ_{l} is large, this approach describes the situations close to local thermodynamic equilibrium (Bruining and Duijn 2006) for the gaseous hydrocarbon mole fraction Y_{h}, i.e., instantaneous vaporization. The vaporization rate W_{v} vanishes under the conditions

$$W_{\mathrm{v}} = 0 \quad \text{when} \quad s_{\mathrm{l}} > 0,\ Y_{\mathrm{h}} = Y_h^{\mathrm{eq}} \text{ or } \ s_{\mathrm{l}} = 0. \tag{2.25}$$

2.1 Initial and Boundary Conditions

The initial reservoir conditions are taken as

$$t = 0,\ x \geq 0: \quad T = T^{\mathrm{ini}},\ \ s_{\mathrm{l}} = s_l^{\mathrm{ini}} R(x),\ \ Y_{\mathrm{h}} = Y_h^{\mathrm{eq}},\ \ Y_{\mathrm{o}} = 0, \quad P_{\mathrm{g}} = P_{\mathrm{ini}}(x). \tag{2.26}$$

where $R(x)$ is a Ramp function. It is necessary for simulation purposes to specify the initial pressure curve $P_{\mathrm{ini}}(x)$. In the entrance domain $0 \leq x < x_e$, where the oil saturation is initially zero, the initial pressure is given by

$$P_{\mathrm{ini}}(x) = P_0 + \mu_{\mathrm{g}} u_{\mathrm{inj}} \left(\frac{x_e - x}{k} + \frac{l - x_e}{k_g(s_{\mathrm{l}}^{\mathrm{ini}})}\right) \tag{2.27}$$

and in the rest of the domain, i.e., for $x_e \leq x \leq l$, where l is the length of the system

$$P_{\mathrm{ini}}(x) = P_0 + \frac{(l - x)\mu_{\mathrm{g}} u_{\mathrm{inj}}}{k_g(s_{\mathrm{l}}^{\mathrm{ini}})}\ . \tag{2.28}$$

We use the parameters from Table 1 and $x_e = 15$ m, $l = 50$ m.

The injection conditions at $x = 0,\ t \geq 0$ are

$$s_{\mathrm{l}} = Y_{\mathrm{h}} = 0, \quad T = T^{\mathrm{ini}}, \quad Y_{\mathrm{r}} = 1 - Y_{\mathrm{o}}^{\mathrm{inj}}, \quad u = u_{\mathrm{inj}}, \quad Y_{\mathrm{o}} = Y_o^{inj}, \tag{2.29}$$

Table 1 Values of reservoir parameters for heptane

$A_r = 4{,}060\ s^{-1}$	$P_0 = 10^6$ Pa	$T^{ini} = 300$ K
$c_g = 29$ J/mol K	$Q_r = 440$ kJ/mol	$u^{inj} = 8.0 \times 10^{-7}$ m/s
$c_l = 224$ J/mol K	$Q_v = 31.8$ kJ/mol	$Y_{inj} = 0.21$
$C_m = 2$ MJ/m ^{3}K	$R = 8.314$ J/mol K	$\lambda = 3$ W/m K
$D_{cap} = 1 \times 10^{-7}$ m^2/s	$s_l^{ini} = 0.9$	$\nu_g = 1.36$ mol/mol
$D_g = 1 \times 10^{-6}$ m^2/s	$s_{lr} = 0.1$	$\nu_l = 0.090$ mol/mol
$k = 10^{-10}$ [m^2]	$T^{ac} = 7{,}066$ K	$\rho_l = 6{,}826$ mol/m^3
$n = 0.5$	$T^{bn} = 371$ K	$\varphi = 0.3$

We use D_{cap} to denote the average capillary diffusion coefficient

corresponding to the injection of an oxidizer (air) at the reservoir temperature. The condition $u = u_{inj}$ leads to an injected flux of $u_{inj}\rho_g$. It is assumed that there are no gaseous hydrocarbons in the injected gas, i.e., $Y_h = 0$. The production conditions at $x = l, t \geq 0$ are

$$\partial_x s_l = \partial_x Y_o = \partial_x Y_r = \partial_x T = 0, \quad P_g = P_0. \tag{2.30}$$

3 Analytical Solution: Wave Sequence Solutions

It is the purpose of this paper to compare numerical to analytical results obtained previously. The analytical expressions are derived with zero molar diffusion, capillary diffusion, and thermal diffusion coefficients. We summarize the results of the analytical solution (Mailybaev et al. 2013) for reasons of easy reference. The analytical solution describes the combustion of a light oil by MTO. Our interest is the behavior at large times. The solution consists of a sequence of waves separated by constant states. As shown in Fig. 1, the solution consists of three waves, i.e., the thermal, MTO, and saturation wave. The thermal wave is the slowest wave due to the high heat capacity of rock. The constant states at the upstream side of the thermal wave are determined by the injection boundary conditions. As shown in Fig. 1 the temperature in the thermal wave changes from $T = T^{ini}$ upstream to some value T^- further downstream. The equation for the calculation of T^- can be found in Mailybaev et al. (2013). The MTO region contains the most interesting traveling waves, possessing the same speed v. In this region, all the dependent variables T, s_l, u, Y_h, Y_o depend on a single

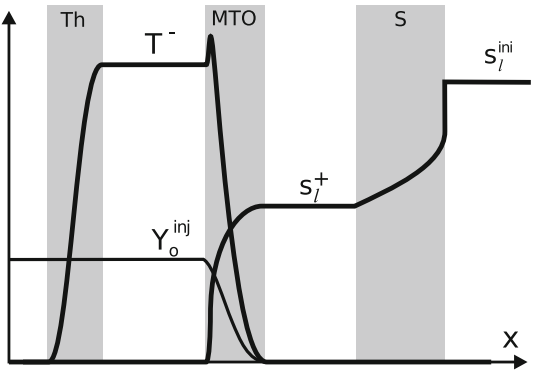

Fig. 1 Wave sequence solutions with the thermal (Th), MTO, and saturation (S) region. Indicated are the distributions of the temperature T, oleic saturation s_l, and oxygen fraction Y_o (Mailybaev et al. 2013)

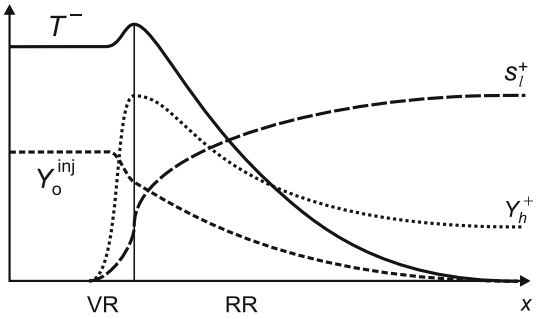

Fig. 2 Schematic graphs of the MTO wave profile. Indicated are changes in the temperature T, liquid fuel saturation s_l, oxygen fraction Y_o, and fuel fraction Y_h in the gas. The *thin* region VR is dominated by vaporization and the much *wider* region RR is dominated by MTO reaction (with slow condensation). The VR is much thinner than the RR, because it is assumed that vaporization rate is much faster than the reaction rate (Mailybaev et al. 2013)

traveling coordinate $\xi = x - vt$, i.e., in a moving frame of reference with speed v the profiles are stationary. Reference Mailybaev et al. (2013) uses the solution of the traveling wave to relate quantities at the upstream side $(T^-, s_l^-, u^-, Y_h^-, Y_o^-)$ to those at the downstream side $(T^+, s_l^+, u^+, Y_h^+, Y_o^+)$. It turns out that the wave speed v can also be obtained from these quantities (Mailybaev et al. 2013). The region upstream of the MTO wave contains injected gas with an oxygen fraction $Y_o^{inj} > 0$ and no gaseous hydrocarbons, $Y_h = 0$. Our interest is in situations where the reaction rate w_r vanishes both at the upstream and downstream sides of the MTO region; we find the condition $s_l = 0$ (no fuel) at the entrance and no oxygen at the production side. Downstream of the MTO wave there are liquid hydrocarbons with saturation $s_l^+ > 0$ and temperature $T = T^{ini}$. The equilibrium conditions $W_r = W_v = 0$ require $Y_o = 0$ and $Y_h = Y_h^{eq}(0)$. Expressions for the five unknown quantities in the limiting states, i.e., T^-, s_l^+, the Darcy velocities u^-, u^+, and the wave speed v of the MTO wave are given in Mailybaev et al. (2013). Finally, the saturation region travels downstream of the MTO wave, see Fig. 1. In this region, the temperature is constant and equal to $T = T^{ini}$. Therefore, we have equilibrium between liquid heptane and heptane vapor, i.e., $Y_h = Y_h^{eq}(T^{ini})$, and there is no net vaporization and condensation. The oxygen has been consumed completely in the MTO region. Therefore, we have $Y_o = 0$ in the saturation region and no reaction occurs. The saturation region contains a Buckley-Leverett solution constructed using the standard procedure involving the Welge tangent construction (Welge 1952). Briefly, from upstream to downstream, it consists of a rarefaction, a shock, and a constant state, see also Oleinik (1959). Recall that in the analytical solution, thermal, mass, and capillary diffusion are disregarded.

We continue to detail the behavior of the MTO region. The mathematical analysis is simplified in an essential way by the physical assumption that the vaporization rate is much faster than the reaction rate. Under this assumption we can divide the wave profile into the vaporization region (VR) and reaction region (RR), see Fig. 2. The VR is very thin, as its width is approximately proportional to the ratio between the reaction and vaporization rates. The surprising feature of MTO is that the thin vaporization region is located upstream of the RR. Here the fraction Y_h of gaseous fuel raises from $Y_h = 0$ in the injected gas to the equilibrium value $Y_h = Y_h^{eq}(T^{res})$ at the downstream end of the VR (see Fig. 2). Since this region is very thin and the reaction rate is not large at the prevailing low fuel concentration, the oxygen consumption is negligible and we neglect the reaction process in the VR. Downstream of the VR, we have the RR. In the RR, most of the MTO reaction occurs, as well as slow

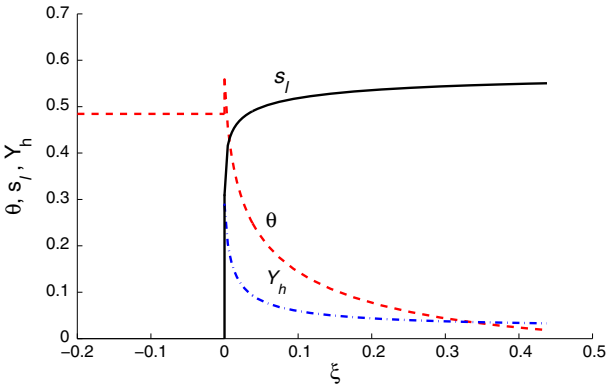

Fig. 3 The blown up analytic diffusionless MTO wave profile for parameters in Tab. 1. The *horizontal* span corresponds to 15 mm. Shown are the variables T, s_l, and Y_h as functions of the dimensionless traveling wave coordinate ξ (the dimensional length scale is $x^* = 0.022\,\mathrm{m}$). The dimensionless quantity $\theta = (T - T^{ini})/(T^b - T^{ini})$ is used to rescale the temperature. The figure was obtained with quadratic permeabilities (Mailybaev et al. 2013), i.e., $k_\mathrm{l} = (s_l - 0.25)^2$ and $k_\mathrm{g} = (1 - s_\mathrm{l})^2$, as opposed to the relative permeability functions (2.12), (2.13), used in our simulations. The very *thin* VR appears as a peak of temperature, see also Fig. 2

condensation due to the temperature decrease in the direction of gas flow. Along the RR, the equilibrium condition $Y_\mathrm{h} = Y_h^{\mathrm{eq}}(T)$ holds approximately.

Plots of the diffusionless analytical profiles shown in Fig. 3 confirm that the form of the wave profile in the RR remains qualitatively similar in the general case, i.e., the variables $T, Y_\mathrm{h}, Y_\mathrm{o}$ decrease in the direction of gas flow in the RR, while s_l increases. The downstream liquid saturation stays around the value $s_\mathrm{l}^+ \approx 0.6$, for a large interval of pressures. Temperature, pressure, and MTO wave speed increase together.

4 Numerical Modeling

We consider a fully coupled, implicit numerical solution approach based on finite elements. We solve the finite-element problem with COMSOL software, which gives numerical results that can be compared to the analytical solution. We apply the mathematical module of COMSOL to introduce the model equations in weak form. We use fifth- order Lagrange elements, which means that the basis functions in this finite element space are polynomials of degree five. In other words, on each mesh element, the solution is a polynomial of degree five and the entire solution is a sum of piecewise fifth-order polynomials. The grid size in the numerical simulation is 0.01 m, which is fine enough to capture the multi-scale processes and is capable of resolving the salient features. The spatial resolution of 5000 is fine enough.

Let us consider reservoir parameters values given in Table 1. The values correspond to heptane (C_7H_{16}) as a fuel. Parameters of the MTO reaction rate vary considerably depending on specific conditions. The availability of reaction rate data is limited. In Table 1, we present the MTO rate parameters compatible with experimental results obtained in Freitag and Verkoczy (2005). In our solutions, the wave speed and limiting states are fortunately weakly dependent on the elusive kinetic parameters.

As shown in Fig. 4, the numerical solution exhibits two regions (thermal and MTO) in the same way as the analytical solution. The saturation region has moved out of sight to the right.

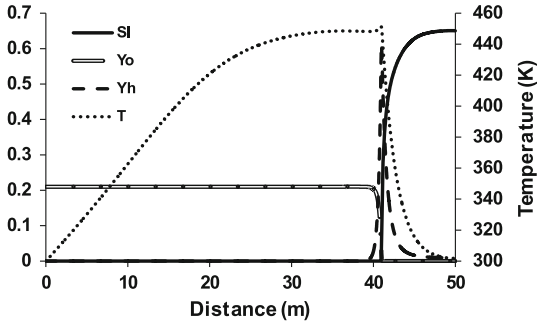

Fig. 4 Wave sequence solution with the thermal and MTO regions. Indicated are the distributions of the temperature T, liquid saturation s_l , oxygen mole fraction Y_o, and gaseous hydrocarbon mole fraction Y_h at $t = 4 \times 10^7$ s in base case related to Table 1. Note near $x = 40$ the abrupt decay of the oxygen concentration, the narrow peak of the Y_h concentration, and the rapid decay in temperature. Consequently, the reaction region (RR) and the vaporization region (VR) are also narrow and partly overlapping

The analytical and numerical solution look similar, in spite of the presence of diffusion terms in the numerical solution. For the parameters used by us, the thermal wave is the slowest wave. Therefore, the thermal wave travels in the region of the reservoir from which the liquid and gaseous hydrocarbons were already displaced, i.e., $s_\mathrm{l} = 0$. Also, $Y_\mathrm{h} = 0$, as the injected gas contains no gaseous hydrocarbons. Therefore, the liquid fractional flow function f_l, the reaction rate w_r, and the evaporation rate w_v are all zero. Since there is no reaction in the upstream part of the MTO wave, the oxygen fraction $Y_\mathrm{o} = Y_o^{\mathrm{inj}}$ is constant. The temperature in the thermal wave changes from the injection value $T = T^{\mathrm{ini}}$ upstream to some value T^- in the plateau. The gradual increase is due to the non-zero value of the thermal conductivity. A steeper increase is illustrated in Fig. 10, where a very low thermal conductivity is used. The Darcy velocity upstream of the thermal wave is the injection Darcy velocity $u = u_{\mathrm{inj}}$. The MTO region contains the most interesting waves in our solution, viz., evaporation and combustion. The saturation region travels downstream of the MTO wave. In this region, the temperature is equal to the initial temperature $T = T^{\mathrm{ini}}$. Downstream of the MTO region there is liquid-gas equilibrium $Y_\mathrm{h} = Y_h^{\mathrm{eq}}(0)$, and there is neither vaporization nor condensation, see (2.24). The oxygen has been consumed completely in the MTO region. No reaction occurs downstream of the MTO region as the oxygen mole fraction is zero ($Y_\mathrm{o} = 0$), see (2.23) and no reaction occurs upstream of the MTO region due to lack of fuel. Since the volume of each phase remains constant, the total Darcy velocity is also constant in regions of constant temperature.

When one compares the analytical (Fig. 3) and numerical computations (Fig. 4), one must keep in mind that different relative permeabilities were used. The width of the reaction region (RR) evaluated by the decline of the oxygen concentration is of the order of one meter in the diffusive simulation as shown in Fig. 4, while the width in the diffusionless analytical solution (Fig. 3) is of the order of millimeters. This discrepancy is due to both physical (molecular, capillary, and thermal diffusion) and numerical diffusion, all present in the simulation. The vaporization rate is made very fast by the application of a high transfer function in the numerical computations or by using thermodynamic equilibrium in the analytical computations. In the RR, the wave profile is characterized by steep changes in all variables at higher temperatures, followed by slower variations at lower temperatures downstream (see Fig. 3). Note also that the temperature T attains a maximum at a peak that determines the resonance state. At this state the heat consuming vaporization at the VR is replaced by the heat

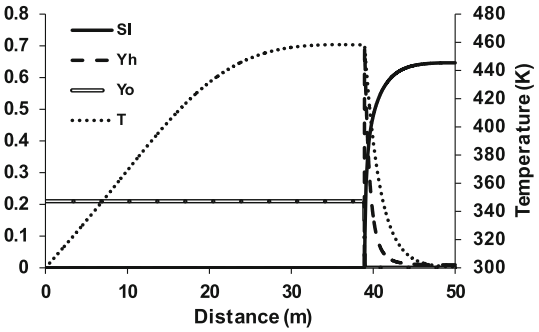

Fig. 5 Wave sequence solution with the thermal and MTO regions. Indicated are the distributions of the temperature T, liquid saturation s_l, oxygen mole fraction Y_o, and the gaseous hydrocarbon mole fraction Y_h at $t = 4 \times 10^7$ s in the case of extremely small gas diffusion, i.e., $D_\mathrm{g} = 1 \times 10^{-9}$ m$^2/s$

providing combustion process in the reaction region (RR). As shown in Fig. 3, the oxygen mole fraction Y_o, the gaseous hydrocarbon mole fraction Y_h, and temperature T change more steeply in the RR wave than the corresponding profiles in Fig. 4. Note that T^- is equal to $T^{ini} + 0.85(T^b - T^{ini})$ in Fig. 4, which means that the temperature at the upstream part of the MTO region T^- is 177^{o}C. This value is between the boiling point T_b and the temperature T^- upstream of the MTO region in Fig. 3. Indeed, the temperature upstream of the MTO region increases to become close to T^b by taking into account the diffusive processes to the model, as was already conjectured in Mailybaev et al. (2013). The liquid saturation downstream of the MTO region, s_l^+ in Fig. 4, is about 0.65 as opposed to 0.56 in the analytical solution.

4.1 Effect of Gas Diffusion

There is no diffusion in the liquid phase, because there is only one component. However, there is diffusion in the gas phase. As stated above we use a single diffusion coefficient in Eq. (2.19). Because diffusion coefficients are usually small, their physical impact can easily be masked by such processes introduced by the numerical models. The finite element code uses algorithms that minimize such processes; diffusion effects are explicitly introduced by adding a diffusion term to the equations. When the injection velocity is small, diffusion effects are well represented by our numerical model. In the base case with a diffusion coefficient $D_\mathrm{g} = 10^{-6}$ m^2/s, as shown in Fig. 4, the effect of diffusion is small. However, it is clearly visible in the oxygen concentration Y_o profile, where the oxygen concentration decreases steeply, but smoothly to zero. The gaseous hydrocarbon profile Y_h is a peak with a finite width. At the upstream side of the MTO region, hydrocarbon evaporates, whereas it condenses at the downstream side. The curve is asymmetric and has a tail, where slow condensation occurs. If we choose a smaller diffusion coefficient, e.g., $D_\mathrm{g} = 10^{-9}$ m^2/s, the oxygen mole fraction shows a much steeper decline (see Fig. 5). The peak representing the gaseous hydrocarbon is much steeper, in particular, at the upstream side of the MTO region. However, the downstream side looks very similar to the case with base diffusion coefficient. Simulations with higher diffusion coefficients ($D_\mathrm{g} = 10^{-5}$ m^2/s) show a slower decline of the oxygen concentration and a hydrocarbon peak that is also slowly increasing at the upstream side of the MTO region, Fig. 6. Moreover, higher diffusion coefficient lowers the maximum temperature and gives rise to a small temperature spike in the evaporation region. The general appearance of the solution is preserved when the gas diffusion is increased within the range of physically accepted values. Within this range, the amount of recovered oil by the MTO region does not change significantly.

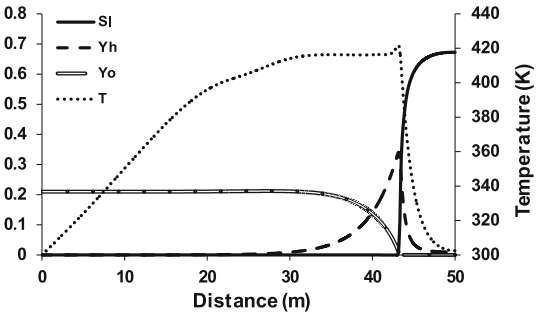

Fig. 6 Wave sequence solution with the thermal and MTO regions. Indicated are the distributions of the temperature T, liquid saturation s_l, oxygen mole fraction Y_o, and gaseous hydrocarbon mole fraction Y_h at $t = 3.4 \times 10^7 sec$ in the case of large gas diffusion $D_g = 1 \times 10^{-5}\ m^2/s$

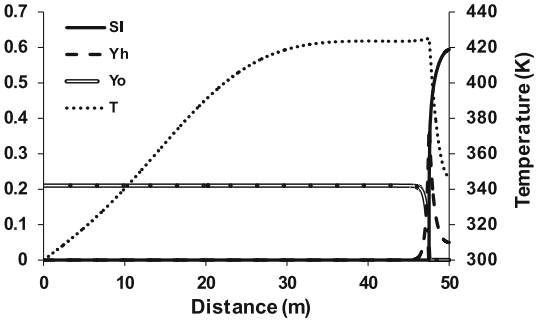

Fig. 7 Wave sequence solution with the thermal and MTO regions. Indicated are the distributions of the temperature T, liquid saturation s_l, oxygen mole fraction Y_o, and gaseous hydrocarbon mole fraction Y_h at $t = 4 \times 10^7$ s in the case of small capillary diffusion $D_{cap} = 1 \times 10^{-10}\ m^2/s$

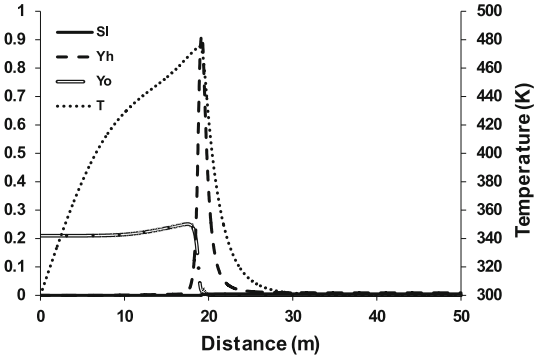

Fig. 8 Wave sequence solution with the thermal and MTO regions. Indicated are the distributions of the temperature T, liquid saturation s_l, oxygen mole fraction Y_o, and gaseous hydrocarbon mole fraction Y_h at $t = 4 \times 10^7$ s in the case of large capillary diffusion $D_{cap} = 1 \times 10^{-4}\ m^2/s$

4.2 Effect of Capillary Pressure

Large capillary forces cause the gas displacement to be the main recovery mechanism and a small amount of oil is left behind for the combustion. As shown by a comparison of Figs. 4 and 7, a lower capillary diffusion leads to a lower temperature and a lower gaseous hydrocarbon concentration (the integrated mole fraction of gaseous hydrocarbon in Fig. 7 is 0.43 m, which is smaller than 0.74 m in Fig. 4). For a higher capillary diffusion (above physically reasonable values), the results of which are displayed in Fig. 8, the temperature is higher and a larger amount of gaseous hydrocarbons (the integrated mole fraction is 1.45 m) are produced. In this case, the liquid saturation is really low, which means that higher capillary forces decrease the amount of oil available for MTO. Large capillary forces decrease the velocity of the MTO region and therefore increase the temperature (see Fig. 8).

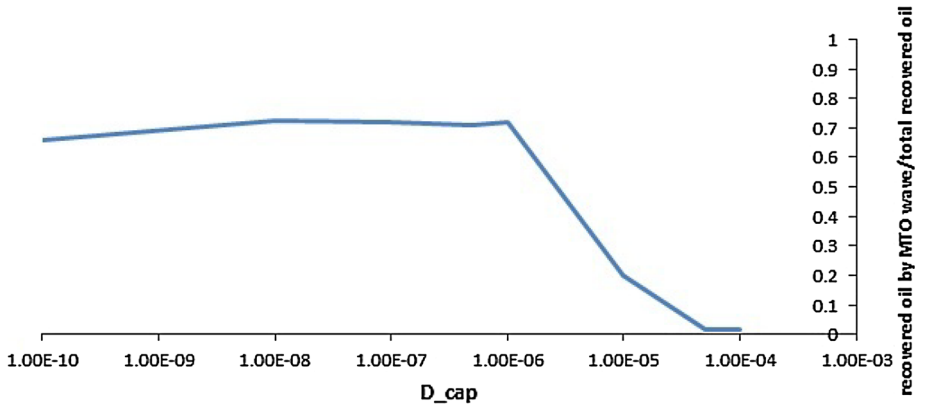

Fig. 9 Effect of capillary diffusion on the amount of oil recovered by the MTO wave

Fig. 10 Wave sequence solution with the thermal and MTO regions. Indicated are the distributions of the temperature T, liquid saturation s_l, oxygen mole fraction Y_o, and gaseous hydrocarbon mole fraction Y_h at $t = 4 \times 10^7$ s in the case of small thermal conductivity $\lambda = 0.03\ W/m\ K$

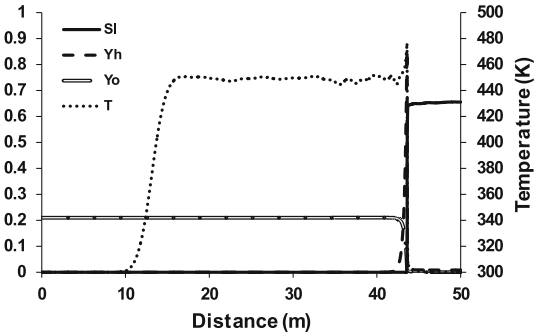

Larger capillary forces sweep more oil ahead of the vaporization/combustion zone. Now the dominant displacement mechanism is capillary mixing away from the MTO region. The smaller amount of oil that enters the MTO region is partly combusted and partly evaporated. Increasing capillary forces enhance recovery by gas displacement and leave less oil behind to be recovered by the vaporization/combustion process (see Fig. 9). There is a continuous change between the relative importance of gas displacement and MTO wave recovery. For high capillary coefficients, which are however, slightly above physically acceptable values, the appearance of the solution changes completely.

4.3 Effect of Thermal Conductivity

Thermal conductivity manifests itself through the value of the quotient of the thermal conductivity and the heat capacity, which is called the thermal diffusion coefficient. The temperature profiles for smaller conductivity (with $\lambda = 0.03\ W/m\ K$, see Fig. 10) show steeper transitions than for the base case values (see Fig. 4). The lower the thermal diffusion coefficient, the thinner the reaction region (RR). For reasons of illustration we took thermal conductivity values that are unrealistically small. The ensuing temperature profile shows numerical fluctuations. At higher thermal conductivity, e.g., with $\lambda = 15\ W/m\ K$ (Fig. 11), we see more smooth transitions. The temperature profile does not show fluctuations. The temperature and hydrocarbon vapor spikes in Fig. 4 widen and flatten for the higher thermal diffusion coefficient.

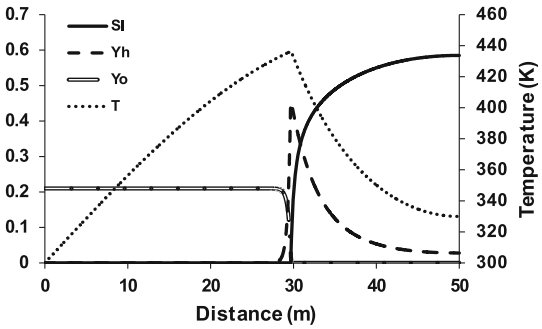

Fig. 11 Wave sequence solution with the thermal and MTO regions. Indicated are the distributions of the temperature T, liquid saturation s_l, oxygen mole fraction Y_o, and gaseous hydrocarbon mole fraction Y_h at $t = 4 \times 10^7$ s in the case of large thermal conductivity $\lambda = 15\ W/m\ K$

We distinguish three aspects. First, there is the rate of oil combustion, which is given by the oxygen injection rate, considering that the oxygen consumption is complete. The velocity of the combustion front is determined by the density of the fuel participating in the reaction process, which is not necessarily related to the amount of oil left behind by the gas displacement process, because part of the oil also evaporates. The oil left behind by the displacement process is removed due to a combination of evaporation and combustion in the MTO region. This can explain why for a higher gas displacement efficiency the velocity of the MTO region can become lower.

5 Conclusions

Air injection with the purpose of improving volatile oil recovery is a method that deserves investigation; it can be modeled as a medium temperature oxidation (MTO) process. A model was proposed to study the effect of diffusive processes (mass, thermal, and capillary) on MTO of light oil in porous media. The proposed two-phase model considers evaporation, condensation, and reaction with oxygen. This model includes three gaseous components (oxygen, gaseous hydrocarbon, and remaining gas), the oil saturation, and an energy balance equations. MTO combustion completely displaces the oil at a cost of small amounts of burned oil. We consider light oil recovery by air injection at medium pressures in a linear geometry, for the case when gas-phase combustion and water are neglected. However, the effect of gas-phase reactions and the presence of water need to be considered in the future.

We used a finite element package (COMSOL) to obtain a numerical solution for comparison with an analytical solution in a zero diffusion model obtained previously (Mailybaev et al. 2013). The numerical model uses fifth-order Lagrangian base functions. Combined with a central difference scheme used in the finite element package, this makes it possible to model situations both at low diffusion and high diffusion coefficients. The numerical model is capable to quantify the effect of the diffusive processes, while the qualitative behavior of the numerical solution is similar to that of the analytical solution. The solution consists of three waves, i.e., a thermal wave, an MTO wave, and a saturation wave, separated by constant state regions. The results show that vaporization occurs upstream of the combustion zone.

The effect of the diffusive terms is as follows. Molecular diffusion lowers the temperature in the MTO region, but creates a small peak in the vaporization region. Capillary diffusion increases the temperature in the upstream part of the MTO region. Higher capillary diffusion increases the recovery by gas displacement and lowers the recovery by the combustion mechanism. The analytical solution, without diffusive terms, and the numerical solution become

completely different at very high capillary diffusion coefficients. The effect of thermal diffusion smoothes the thermal wave and widens the hydrocarbon vapor peak.

Acknowledgments This research was carried out within the context of the ISAPP Knowledge Centre. ISAPP (Integrated Systems Approach to Petroleum Production) is a joint project of the Netherlands Organization of Applied Scientific Research TNO, Shell International Exploration and Production, and Delft University of Technology. The paper was also supported by Grants of PRH32(ANP 731948/2010, PETROBRAS 6000.0061847.10.4), FAPERJ(E-26/102.965/2011, E-26/111.416/2010, E-26/110.658/ 2012, E-26/110.237/2012, E-26/111.369/2012) and CNPq (301564/2009-4,472923/2010-2, 477907/2011-3, 305519/2012-3, 402299/2012-4, 470635/2012-6) and Capes/Nuffic 024/2011. The authors thank TU Delft and IMPA for providing the opportunity for this work.

References

Abou-Kassem, J.H., Farouq, A., Ferrer, S.M.: Appraisal of steamflood models. J. Rev. Tec. Ing. **9**, 45–58 (1986)

Adagülü, G., Akkutlu, I.: Influence of in-situ fuel deposition on air injection and combustion. J. Can. Pet. Technol. **46**(4), 54–61 (2007)

Akin, S., Kok, M.V., Bagci, S., Karacan, O.: Oxidation of heavy oil and their SARA fractions: its role in modeling in-situ combustion. SPE 63230 (2000).

Bakry, A., Al-Salaymeh, A., Al-Muhtaseb, A.H., Abu-Jrai, A., Trimis, D.: Adiabatic premixed combustion in a gaseous fuel porous inert media under high pressure and temperature: Novel flame stabilization technique. Fuel **90**(2), 647–658 (2011)

Bamford, C.H., Tipper, C.E.H.: Comprehensive Chemical Kinetics. Gas-phase Combustion. Elsevier, New York (1977)

Barzin, Y., Moore, R., Mehta, S., Mallory, D., Ursenbach, M., Tabasinejad, F.: Role of vapor phase in oxidation/combustion kinetics of high-pressure air injection (HPAI). In: SPE 135641 (2010).

Barzin, Y., Moore, R., Mehta, S., Ursenbach, M., Tabasinejad, F.: Impact of distillation on the combustion kinetics of high pressure air injection (HPAI). In: SPE 129691-Improved Oil Recovery Symposium (2010).

Bayliss, A., Matkowsky, B.J.: From traveling waves to chaos in combustion. SIAM J. Appl. Math. **54**, 147–174 (1994)

Bear, J.: Dynamics of Fluids in Porous Media. Dover Publications Inc, Dover (1972)

Belgrave, J.D.M., Moore, R.G.: A model for improved analysis of in-situ combustion tube tests. J. Pet. Sci. Eng. **8**(2), 75–88 (1992)

Bird, R.B., Stewart, W.E., Lightfoot, E.N.: Transport Phenomena. Wiley, New York (2002)

Bruining, J., van Duijn, C.J.: Traveling waves in a finite condensation rate model for steam injection. Comput. Geosci. **10**(4), 373–387 (2006)

Bruining, J., Mailybaev, A.A., Marchesin, D.: Filtration combustion in wet porous medium. SIAM J. Appl. Math. **70**, 1157–1177 (2009)

Castanier, L.M., Brigham, W.E.: Modifying in-situ combustion with metallic additives. Situ **21**(1), 27–45 (1997)

Castanier, L.M., Brigham, W.E.: Upgrading of crude oil via in situ combustion. J. Pet. Sci. Eng. **39**, 125–136 (2003)

Dietz, D.N., Weijdema, J.: Wet and partially quenched combustion. J. Pet. Technol. **20**, 411–415 (1968)

Eftekhari, A.A., Van Der Kooi, H., Bruining, J.: Exergy analysis of underground coal gasification with simultaneous storage of carbon dioxide. Energy **45**(1), 729–745 (2012)

Fassihi, M., Brigham, W., Ramey Jr, H.: Reaction kinetics of in-situ combustion: Part 1-observations. Old SPE J. **24**(4), 399–407 (1984)

Fickett, W., Davis, W.C.: Detonation: Theory and Experiment. Dover, Mineola (2011)

Fisher, E.M., Pitz, W.J., Curran, H.J., Westbrook, C.K.: Detailed chemical kinetic mechanisms for combustion of oxygenated fuels. Proc. Combust. Inst. **28**(2), 1579–1586 (2000)

Freitag, N.P., Verkoczy, B.: Low-temperature oxidation of oils in terms of SARA fractions: why simple reaction models don't work. J. Can. Pet. Technol. **44**(3), 54–61 (2005)

Germain, P., Geyelin, J.L.: Air injection into a light oil reservoir: the Horse Creek project. In: Middle East Oil Show and Conference, SPE-37782-MS (1997).

Gerritsen, M., Kovscek, A., Castanier, L., Nilsson, J., Younis, R., He, B.: Experimental investigation and high resolution simulator of in-situ combustion processes; 1. Simulator design and improved combustion

with metallic additives. In: SPE International Thermal Operations and Heavy Oil Symposium and Western Regional Meeting, SPE-86962-MS (2004).
Greaves, M., Ren, S., Rathbone, R., Fishlock, T., Ireland, R.: Improved residual light oil recovery by air injection (LTO process). J. Can. Pet. Technol. **39**(1) ISSN0021-948 (2000).
Greaves, M., Young, T.J., El-Usta, S., Rathbone, R.R., Ren, S.R., Xia, T.X.: Air injection into light and medium heavy oil reservoirs: combustion tube studies on west of shetlands clair oil and light australian oil. Chem. Eng. Res. Des. **78**(5), 721–730 (2000)
Gutierrez, D., Skoreyko, F., Moore, R., Mehta, S., Ursenbach, M.: The challenge of predicting field performance of air injection projects based on laboratory and numerical modelling. J. Can. Pet. Technol. **48**(4), 23–33 (2009)
Hardy, W.C., Fletcher, P.B., Shepard, J.C., Dittman, E.W., Zadow, D.W.: In-situ combustion in a thin reservoir containing high-gravity oil. J. Pet. Technol., SPE-3053-PA, **24**(2), 199–208 (1972).
Helfferich, F.G.: Kinetics of Multistep Reactions, vol. 40. Elsevier Science Limited, Amsterdam (2004)
Khoshnevis Gargar, N., Achterbergh, N., Rudolph-Flöter, S., Bruining, H.: In-Situ oil combustion: processes perpendicular to the main gas flow direction. In: SPE Annual Technical Conference and Exhibition, volume SPE 134655-MS (2010).
Kok, M.V., Karacan, C.O.: Behavior and effect of SARA fractions of oil during combustion. SPE Reserv. Eval. Eng. **3**, 380–385 (2000)
Kulikovskii, A.G., Pashchenko, N.T.: Propagation regimes of self-supported light-detonation waves. Fluid Dyn. **40**(5), 818–828 (2005)
Levenspiel, O.: Chemical Reaction Engineering. Wiley, New York (1999)
Lin, C.Y., Chen, W.H., Lee, S.T., Culham, W.E.: Numerical simulation of combustion tube experiments and the associated kinetics of in-situ combustion processes. SPE J. **24**, 657–666 (1984)
Lin, C.Y., Chen, W.H., Culham, W.E.: New kinetic models for thermal cracking of crude oils in in-situ combustion processes. SPE Reserv. Eng. **2**, 54–66 (1987)
Mailybaev, A.A., Bruining, J., Marchesin, D.: Analysis of in situ combustion of oil with pyrolysis and vaporization. Combust. Flame **158**(6), 1097–1108 (2011)
Mailybaev, A.A., Marchesin, D., Bruining, J.: Resonance in low-temperature oxidation waves for porous media. SIAM J. Math. Anal. **43**, 2230 (2011)
Mailybaev, A.A., Marchesin, D., Bruining, J.: Recovery of light oil by medium temperature oxidation. Transp. Porous Media **97**(3), 317–343 (2013)
Matkowsky, B.J., Sivashinsky, G.: Propagation of a pulsating reaction front in solid fuel combustion. SIAM J. Appl. Math. **35**, 465–478 (1978)
Oleinik, O.A.: Construction of a generalized solution of the cauchy problem for a quasi-linear equation of first order by the introduction of vanishing viscosity. Uspekhi Matematicheskikh Nauk **14**(2), 159–164 (1959)
Peaceman, D.W.: Fundamentals of Numerical Reservoir Simulation, vol. 6. Elsevier, New York (1977)
Pereira, F.M., Oliveira, A.A.M., Fachini, F.F.: Asymptotic analysis of stationary adiabatic premixed flames in porous inert media. Combust. Flame **156**(1), 152–165 (2009)
Poling, B.E., Prausnitz, J.M., John Paul, O.C., Reid, R.C.: The Properties of Gases and Liquids. McGraw-Hill, New York (2001).
Prigogine, I.: Introduction to Non-equilibrium Thermodynamics. Wiley, New York (1962)
Sanmiguel, J., Mallory, D., Mehta, S., Moore, R.: Formation heat treatment process by combustion of gases around the wellbore. J. Can. Pet. Technol. **41**(8) ISSN0021-9487 (2002).
Schott, G.L.: Kinetic studies of hydroxyl radicals in shock waves. III. The OH concentration maximum in the hydrogen-oxygen reaction. J. Chem. Phys. **32**, 710 (1960)
Schult, D.A., Matkowsky, B.J., Volpert, V.A., Fernandez-Pello, A.C.: Forced forward smolder combustion. Combust. Flame **104**, 1–26 (1996)
Schulte, W.: Challenges and strategy for increased oil recovery. In: International Petroleum Technology Conference, Doha, Qatar (2005).
Sharpe, G.J., Falle, S.: One-dimensional nonlinear stability of pathological detonations. J. Fluid Mech. **414**(1), 339–366 (2000)
von Rosenberg, D.U.: Methods for the Numerical Solution of Partial Differential Equations, vol. 16. American Elsevier, New York (1969)
Wahle, C.W., Matkowsky, B.J., Aldushin, A.P.: Effects of gas-solid nonequilibrium in filtration combustion. Combust. Sci. Tech. **175**, 1389–1499 (2003)
Welge, H.J.: A simplified method for computing oil recovery by gas or water drive. Trans. AIME **195**, 91–98 (1952)
Whitham, G.B.: Non-linear dispersion of water waves. J. Fluid Mech. **27**(02), 399–412 (1967)
Whitham, G.B.: Linear and Nonlinear Waves, vol. 42. Wiley-Interscience, New York (2011)

Wood, W.W., Salsburg, Z.W.: Analysis of steady-state supported one-dimensional detonations and shocks. Phys. Fluids **3**, 549–566 (1960)
Xu, Z., Jianyi, L., Liangtian, S., Shilun, L., Weihua, L.: Research on the mechanisms of enhancing recovery of light-oil reservoir by air-injected low-temperature oxidation technique. Nat. Gas Ind. **24**, 78–80 (2004)
Zheng, C.H., Cheng, L.M., Li, T., Luo, Z.Y., Cen, K.F.: Filtration combustion characteristics of low calorific gas in sic foams. Fuel **89**(9), 2331–2337 (2010)